doi:10.1016/j.jmb.2012.06.040 J. Mol. Biol. (2012) 423, 217–231

Contents lists available at www.sciencedirect.com

Journal of Molecular Biology

journal homepage: http://ees.elsevier.com.jmb

Development of the Structural Core and of Conformational Heterogeneity during the Conversion of Oligomers of the Mouse Prion Protein to Worm-like Amyloid Fibrils

Jogender Singh, A. T. Sabareesan, M. K. Mathew and Jayant B. Udgaonkar*

National Centre for Biological Sciences, Tata Institute of Fundamental Research, Bangalore 560065, India

Received 22 April 2012;
received in revised form
15 June 2012;
accepted 28 June 2012
Available online
9 July 2012

Edited by R. Wetzel

Keywords:
prion protein;
oligomers;
hydrogen exchange;
mass spectrometry;
lipid membrane

Understanding how structure develops during the course of amyloid fibril formation by the prion protein is important for understanding prion diseases. Determining how conformational heterogeneity manifests itself in the fibrillar and pre-fibrillar amyloid aggregates is critical for understanding prion strain phenotypes. In this study, the formation of worm-like amyloid fibrils by the mouse prion protein has been characterized structurally by hydrogen–deuterium exchange coupled to mass spectrometry. The structural cores of these fibrils and of the oligomer on the direct pathway of amyloid fibril formation have been defined, showing how structure develops during fibril formation. The structural core of the oligomer not on the direct pathway has also been defined, allowing the delineation of the structural features that make this off-pathway oligomer incompetent to directly form fibrils. Sequence segments that exhibit multiple local conformations in the three amyloid aggregates have been identified, and the development of structural heterogeneity during fibril formation has been characterized. It is shown that conformational heterogeneity is not restricted to only the C-terminal domain region, which forms the structural core of the aggregates; it manifests itself in the N-terminal domain of the protein as well. Importantly, all three amyloid aggregates are shown to be capable of disrupting lipid membrane structure, pointing to a mechanism by which they may be toxic.

Introduction

The self-propagating conversion of the monomeric and α-helix-rich prion protein, PrP^{C} (cellular prion protein), into the disease-causing oligomeric and β-sheet-rich isoform, PrP^{Sc} (scrapie PrP), is known to be the key molecular event in prion disease.[1–5] The structure of PrP^{Sc} is poorly understood, as reflected in three very different models being proposed to describe its structure[6]: the β-helix model,[7] the spiral model,[8] and the parallel in-register β-sheet model.[9,10] Its core region is, however, known to be formed mainly by the C-terminal region of PrP and is

*Corresponding author. E-mail address: jayant@ncbs.res.in.

Abbreviations used: PrP^{C}, cellular prion protein; PrP^{Sc}, scrapie PrP; PrP, prion protein; moPrP, mouse prion protein; HDX, hydrogen–deuterium exchange; MS, mass spectrometry; AFM, atomic force microscopy; ThT, thioflavin T; BLM, black lipid membrane; GdnHCl, guanidine hydrochloride; PEG, polyethylene glycol.

involved in β-sheet formation[9–13] in the cross-β spine characteristic of all amyloid protein aggregates. The molecular details of the transformation of PrP^{C} to PrP^{Sc} are yet to be understood, but it appears that monomeric PrP^{C} partially unfolds first and then subsequently refolds into the oligomeric aggregated form.[4] Structural characterization of the prion protein aggregation pathway has been impeded by the conformational heterogeneity inherent in the aggregation reaction, but this conformational heterogeneity is itself important to delineate because differently structured prion amyloid aggregates form the basis of prion strains that differ in their infectiousness and disease phenotype.[14–16]

Much has been learnt about prion protein aggregation from studies of the aggregation of recombinant prion proteins.[15,17,18] Mechanical agitation of monomeric protein (PrP) destabilized by denaturants leads directly to the formation of straight 8- to 10-nm-wide fibrils at physiological pH.[19] However, at low pH, β-rich oligomers form[19] and go on to generate worm-like fibrils, about 2 nm in diameter, independent of both denaturant and agitation.[20] It seems that the protonation of critical residues leads to the formation of an amyloidogenic conformation by destabilization of the native structure. Since the protonated amyloidogenic conformation is sparsely populated at neutral pH, aggregation to form worm-like fibrils is very slow, and the fibrils are undetectable over an experimental time scale of days. The slowness of the aggregation of such protonated amyloidogenic conformations may be physiologically relevant, because several neurodegenerative diseases, including the prion diseases, are late-onset diseases.

For many proteins associated with amyloid fibril-related diseases, it appears that spherical oligomers and protofibrils (which the worm-like fibrils resemble) are the toxic entities.[21–23] However, fibrils can also be toxic, especially when fragmented.[24] For the prion protein, 300- to 600-kDa oligomers derived from protease-resistant prion aggregates appear to be the most infectious species in prion disorders.[25] Straight fibrils formed *in vitro* have been reported to be toxic,[26] but so have oligomers and/or protofibrillar forms, *in vitro*[27] as well as *in vivo*.[28] Notably, although PrP pathogenesis involves conversion of PrP^{C} to PrP^{Sc}, accumulation of PrP^{Sc} is not correlated with PrP pathogenesis.[29] On the other hand, prion disease susceptibility appears to correlate with the propensity of the protein to form β-rich oligomers.[30] It remains to be established whether the β-rich oligomers and the worm-like fibrils they form are toxic by possessing the capability to disrupt membrane structure.

Previous studies from this laboratory have shown that the β-rich oligomers formed by the full-length recombinant mouse prion protein (moPrP) are composed of two subpopulations of oligomers, the small oligomer S and the large oligomer L.[31,32] Oligomer L was shown to be the direct precursor of worm-like fibrils, while oligomer S appeared to be an off-pathway oligomer.[32] The structural differences between oligomers L and S were not identified, and the internal structure of worm-like fibrils was not known. Since the toxicity of PrP aggregates depends both on their size and on their molecular structure,[33] it becomes important to characterize the structures and toxicities of both oligomers L and S, and of the worm-like fibrils, as well as to determine how structure develops as oligomer L transforms into worm-like fibrils.

In the present study, hydrogen–deuterium exchange (HDX) measurements were carried out in conjunction with mass spectrometry (MS) to characterize the structural cores of all three aggregate forms—oligomer L, oligomer S, and the worm-like fibrils. It is shown that the C-terminal region (sequence segment 170–220) of the protein forms the core regions of both oligomer S and oligomer L, with subtle differences between the two, and that the formation of worm-like fibrils is linked with the expansion of the core region. It is also seen that sequence segments 109–132 and 154–167 are structured, albeit with lower stability than the core region in a significant fraction of the prion molecules in all three aggregates, and that sequence segment 32–55 is structured, again with lower stability, in a significant fraction of the prion molecules in the worm-like fibrils but not in the oligomers. The formation of worm-like fibrils leads to gain in and expansion of heterogeneity in conformation. Finally, it is shown, by monitoring current across black lipid membranes (BLMs) and the swelling of proteoliposomes, that all three aggregate forms are capable of disrupting membrane integrity.

Results

The full-length recombinant moPrP forms β-rich oligomers in aggregation buffer (50 mM glycine and 150 mM NaCl, pH 2) at 25 °C, which then form worm-like fibrils, as seen in an atomic force microscopy (AFM) image (Fig. 1a). Worm-like fibril formation is very slow at 25 °C but is accelerated at elevated temperatures, and Fig. 1b and c shows that at 50 °C, it occurs with exponential kinetics that are probe dependent: the observed rates are 1.35, 0.90, and 0.53 h^{-1}, when monitored using thioflavin T (ThT) fluorescence, mean hydrodynamic radius, and weight-averaged molar mass, respectively. This observation suggests that conformational conversion and fibril growth do not occur concurrently, in agreement with previous results.[20,31]

Multiple structural probes identify on-pathway and off-pathway oligomers

Two subpopulations of the β-rich oligomer[32] could be purified using size-exclusion chromatography

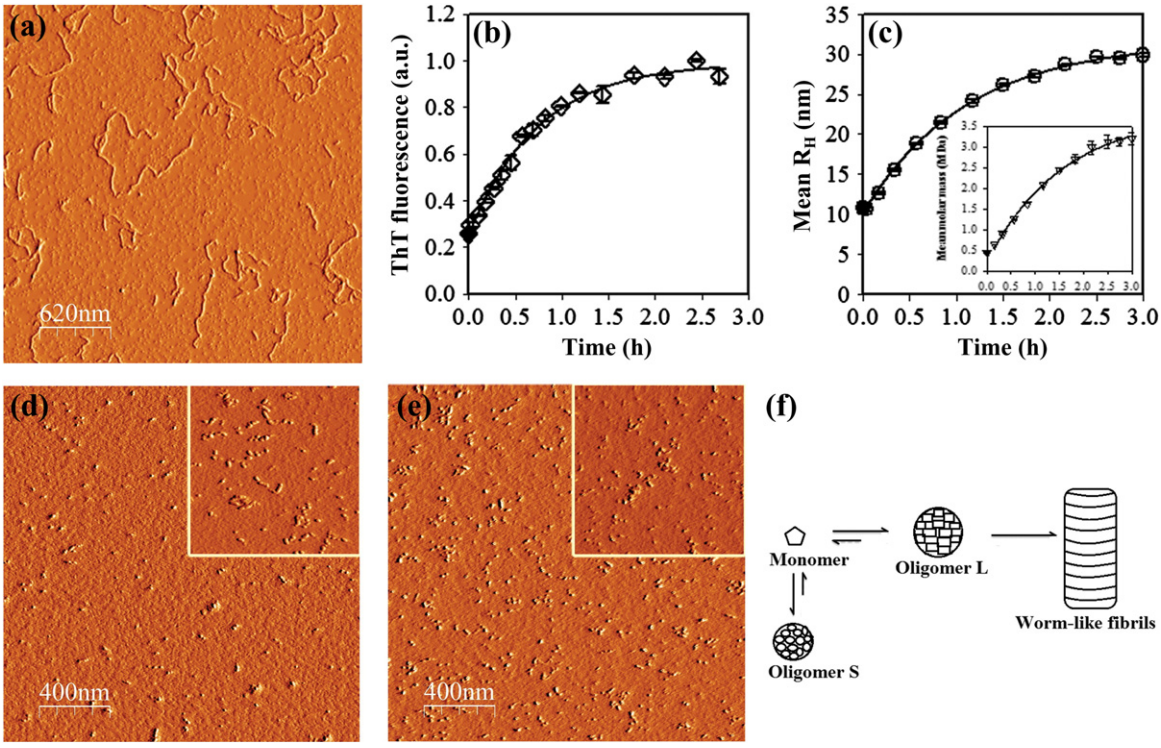

Fig. 1. Worm-like fibril formation at pH 2, 50 °C. (a) AFM image of worm-like fibrils formed at 3 h in the amplitude mode. The worm-like fibrils are about 2 nm wide. The kinetics of worm-like fibril formation by 25 μM protein are shown in (b) and (c). (b) ThT fluorescence-monitored kinetics; (c) mean R_H-monitored kinetics. The inset in (c) shows the weight-averaged molar-mass-monitored kinetics. (d) AFM image of oligomer L at 1 h of purification. The inset in (d) shows the AFM image of oligomer L at 24 h after purification. (e) AFM image of oligomer S at 1 h of purification. The inset in (e) shows the AFM image of oligomer S at 24 h after purification. In (d) and (e), the scale bar is the same for the insets and the main images and the images are in amplitude mode. (f) Scheme describing the formation of worm-like fibrils, showing the on-pathway and off-pathway roles assigned to oligomers L and S, respectively, on the basis of previous kinetic studies[32] and present AFM studies.

(Fig. S1a; Materials and Methods). Incubation of oligomer S in aggregation buffer at 25 °C at concentrations above 5 μM for over 24 h does not result in transformation to either oligomer L or monomer, as detected by size-exclusion chromatography. Figure S1b shows that this is also true for oligomer L, at concentrations greater than 25 μM. AFM images of mature worm-like fibrils taken after incubation for 3 h at 50 °C reveal no oligomers (Fig. 1a). Furthermore, a 300-kDa cutoff filter passed no protein at the end of the aggregation reaction of 25 μM protein, while separate experiments showed that the β-rich oligomers pass freely through the filter and that worm-like fibrils are fully retained (data not shown). Hence, it is straightforward to obtain purified samples of all three amyloid aggregates, for structural characterization as well as for characterization of their toxicities.

The purified oligomers S and L and the worm-like fibrils differ substantially in their molar masses and in their mean hydrodynamic radii, as determined by static light scattering measurements and dynamic light scattering measurements, respectively (Table S1). AFM measurements show that both oligomers L and S are nearly spherical when observed immediately upon purification (Fig. 1d and e), with similar diameters of ~2 nm. Twenty-four hours after purification, however, oligomer L—but not oligomer S—has begun to elongate (Fig. 1d and e, insets). Oligomers L and S differ in their secondary structure as inferred from their far-UV circular dichroism (CD) spectra. The CD spectrum of oligomer S does not change over a 24-h period, while that of oligomer L becomes more like that of the worm-like fibrils (Fig. S1c). Both oligomers bind ThT to the same extent immediately upon purification, but oligomer L shows an increased ThT binding over a 24-h period whereas oligomer S shows no change (data not shown). Static light scattering experiments showed that the molar mass of oligomer L increases over a 24-h period but that of oligomer S is unchanged (Table S1). These observations directly support the previous conclusion from kinetic studies[32] that oligomer L is populated on the pathway and oligomer S off the pathway of worm-like fibril formation (Fig. 1f).

moPrP contains eight Trp residues, seven of which are in the N-terminal half of the sequence. This

region of the sequence is known to be unstructured in native moPrP. Unsurprisingly, the fluorescence spectrum of native moPrP shows an emission maximum at 355 nm as expected for fully hydrated Trp residues, suggesting that the C-terminal Trp is also solvent exposed (Fig. S1d). Figure S1d shows that the fluorescence emission spectra of all three aggregated forms have emission maxima at 355 nm, suggesting that the N-terminal halves of the protein molecules in all three aggregates remain unstructured. More sequence-specific information was then obtained using HDX–MS.

Peptide mapping of moPrP

In HDX–MS studies, the amide hydrogen sites that are protected against HDX can be localized to specific segments of the protein sequence by proteolytic fragmentation at low pH, after the HDX reaction is complete. A peptide map of moPrP was first generated by controlled proteolysis by pepsin at low pH (Fig. S2), as described in Materials and Methods. A total of 26 peptides, which displayed good signal-to-noise ratio in their mass spectra, were identified. These peptides, some of which overlap, cover ~97% of the entire moPrP sequence; the only gap encompasses residues 175–181.

HDX–MS characterization of the cores of the amyloid aggregates

HDX of all three amyloid aggregates, as well as of native protein as a reference, was carried out as described in Materials and Methods. When the three

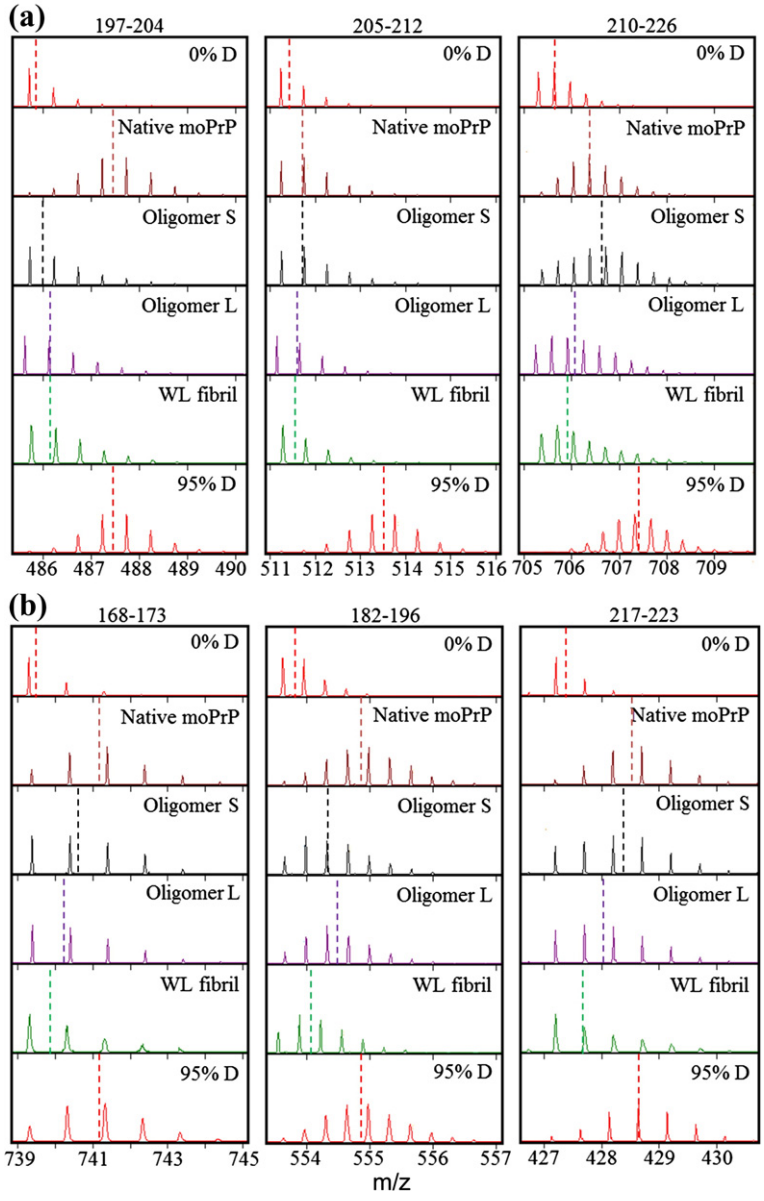

Fig. 2. Mass spectra for selected peptides derived from native moPrP, oligomer S, oligomer L, and worm-like fibril (WL fibril) at 24 h of HDX, along with controls of protonated (0% D) and deuterated (95% D) peptides. The broken lines represent the centroid average m/z for the given peptide. (a) Selected peptides showing protection in oligomer S, oligomer L, and worm-like fibril. (b) Selected peptides showing relatively higher protection in worm-like fibrils compared to oligomer S and oligomer L.

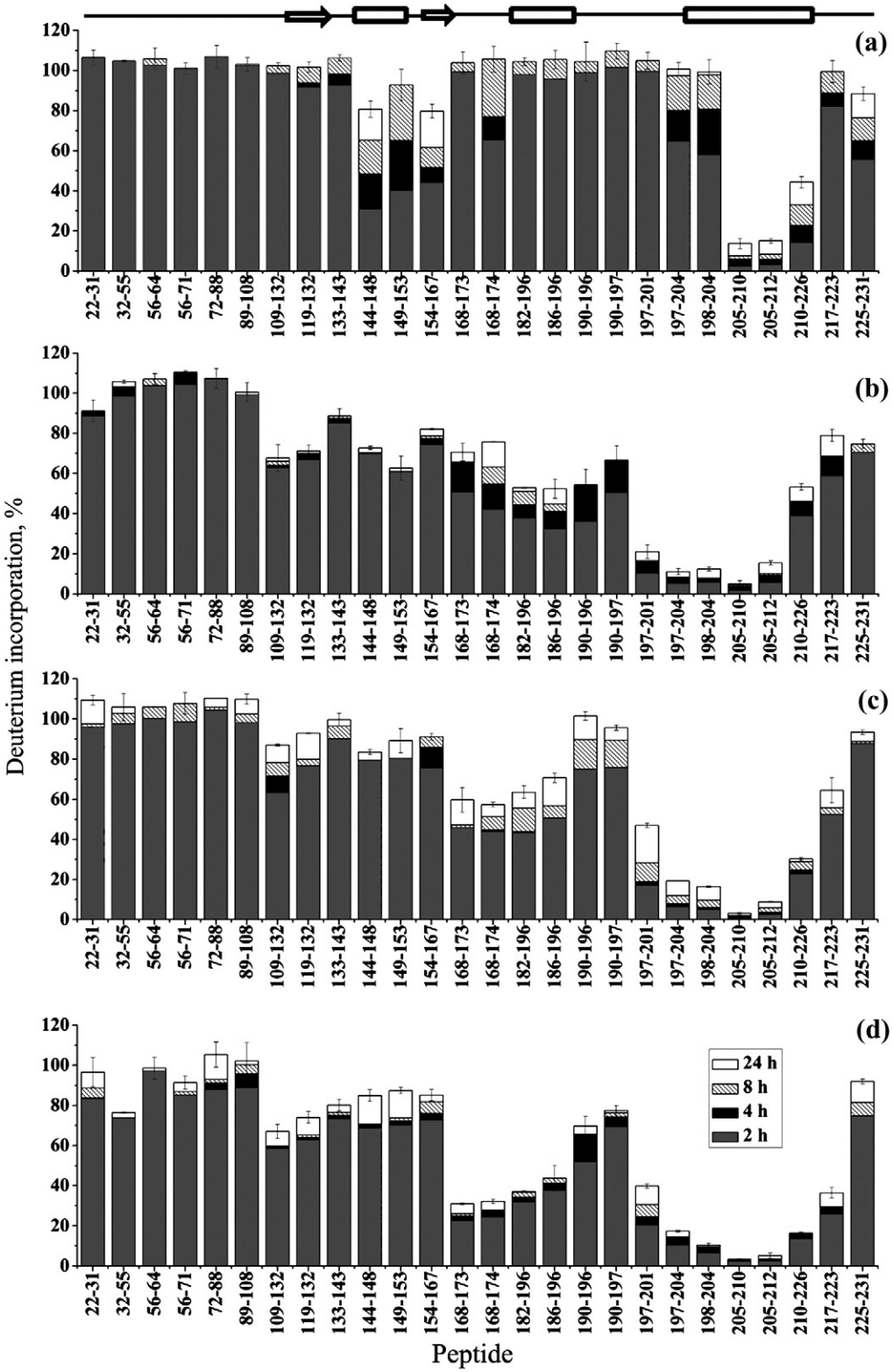

Fig. 3. Deuterium incorporation into different sequence segments of monomeric native moPrP (a), oligomer S (b), oligomer L (c), and worm-like fibrils (d). Stacked bars represent the duration of HDX labeling: 2 h (dark gray), 4 h (black), 8 h (diagonal lines), and 24 h (white), as shown in (d). The percent deuterium incorporation into each peptic fragment was determined from its mass calculated from the overall centroid of the isotopic envelope in the mass spectrum, relative to the mass of the corresponding peptide in 95% D_2O (see Materials and Methods for details). The amino acid residue 22 at the N-terminus is Met. Error bars represent the standard deviations from three independent experiments.

amyloid aggregates, as well as the native protein as a reference, were allowed to undergo HDX for 24 h, the mass spectra of the peptide fragments generated from them display unimodal isotope distribution patterns (Fig. 2), indicating that each fragment exists primarily in a single conformation. For each protein aggregate, different fragments have undergone deuterium incorporation to different extents. This indicates that the sequence segments, from which the fragments originate, differ in their structural content and hence in the protection they afford against HDX. The same sequence segment also sometimes incorporates deuterium to different extents in different aggregates. For example, little deuterium incorporates into the sequence segment 197–204 of the oligomers and worm-like fibrils, but the same segment of native protein displays full incorporation, indicating that this sequence segment is protected in the aggregates, but is unprotected in native protein. Figure 2a shows some of the sequence segments that are relatively structured in all three aggregates, while Fig. 2b shows sequence segments that are relatively more structured in the worm-like fibrils than in either oligomer. The mass spectra shown in Fig. 2 are for fragments derived from the C-terminal half of the sequence, whose different segments are differentially protected in the different protein forms. In contrast, the N-terminal half of the sequence does not appear to have any protective structure in any of the four protein forms: all peptide fragments derived from this half of the sequence become more than 75% deuterated after 24 h of HDX (data not shown).

Figures S3–S5 show mass spectra of fragments corresponding to different sequence segments of worm-like fibrils, oligomer L, and oligomer S, respectively, after each protein form was allowed to undergo HDX for different periods of time. Monitoring the time course of increasing mass during the HDX reaction allows for the estimation of the stabilities of the protective structure in each sequence segment. There is little, if any, increase in deuterium incorporation from 2 to 24 h into fragments from the C-terminal half that exhibit unimodal isotope distribution patterns, indicating that the protective structures are stable against exchange.

Delineating the structural cores of both oligomers and of the worm-like fibrils

The extent of deuterium incorporation into different sequence segments of native moPrP and of the three aggregates at different times of HDX is summarized in Fig. 3. For native moPrP, the regions of lowest deuterium incorporation (segments 144–167 and 205–220) correspond to the most protected segments of structure, which are helix 1, β-strand 2, and helix 3. In the case of the aggregates, however, the organization of secondary structure is not known. The most protected regions are assumed to correspond to the structural cores of the aggregates, where protection at the amide hydrogen sites arises due to the hydrogen-bonding characteristic of the β-sheet structure.

The basic structural cores of the three aggregated forms are in the C-terminal region, particularly in

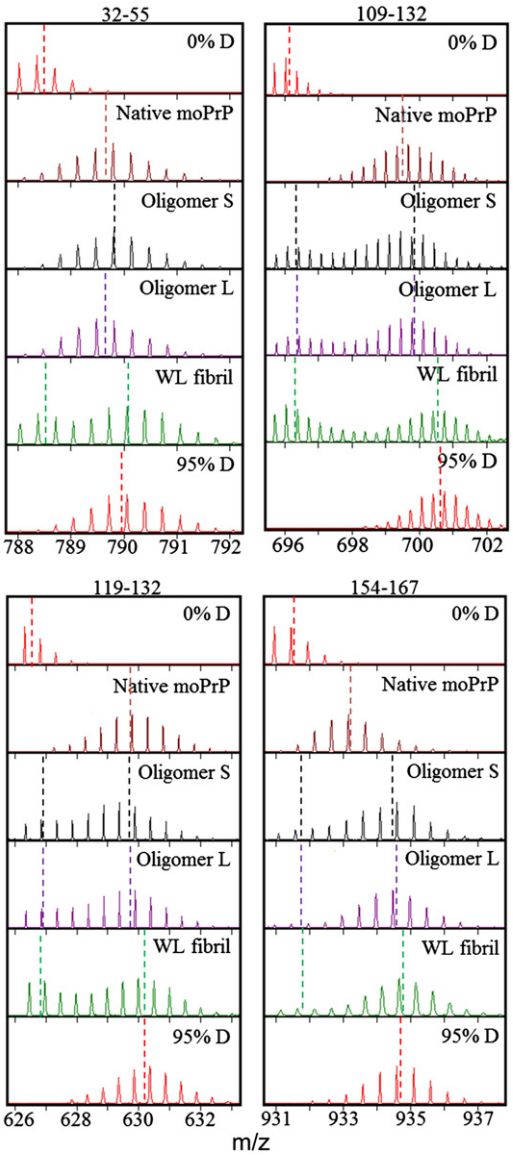

Fig. 4. Conformational heterogeneity in oligomer S, oligomer L, and worm-like fibrils. Mass spectra of selected peptides showing bimodal mass distributions for oligomer S, oligomer L, and worm-like fibril (WL fibril) at 4 h of HDX, along with controls of protonated (0% D) and deuterated (95% D) peptide fragments. Peptide 32–55 shows a bimodal mass distribution only for worm-like fibrils. Single broken lines represent the centroid average m/z for the given peptide. Two broken lines for one peptide fragment represent the centroid average m/z values for the protected (lower m/z) and unprotected forms (higher m/z).

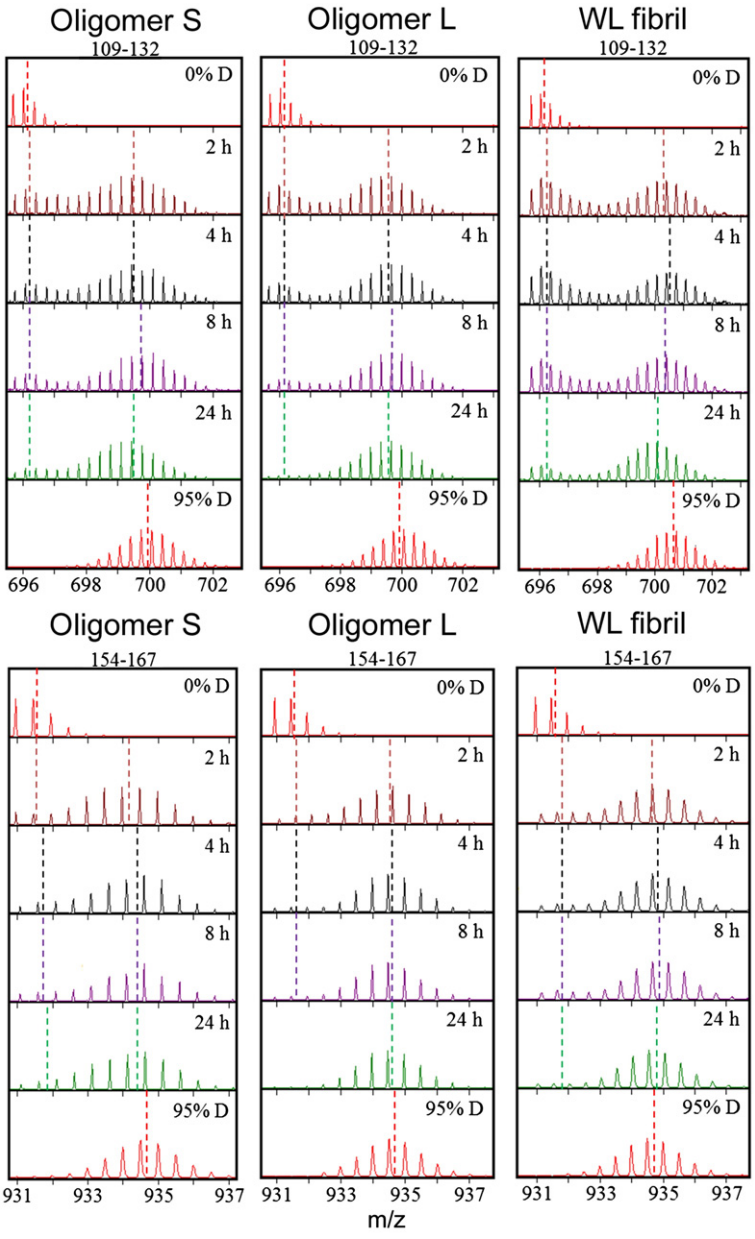

Fig. 5. Relative conformational heterogeneity in oligomer S, oligomer L, and worm-like fibrils. Mass spectra of selected peptides showing bimodal mass distributions for oligomer S, oligomer L, and worm-like fibril (WL fibril) at different times of HDX, along with controls of protonated (0% D) and deuterated (95% D) peptide fragments. Single broken lines represent the centroid average m/z for the given peptide. Two broken lines for one peptide fragment represent the centroid average m/z values for the protected (lower m/z) and unprotected forms (higher m/z).

sequence segment 168–223, but there are subtle differences among the three core regions. One difference is in the boundaries of the structural core regions. The core region boundary for oligomer S extends up to residue 216 at the C-terminal region while the N-terminal boundary is not well defined due to the gap between residues 175–181 in the peptide map. Peptides C-terminal to the gap show protection while peptides N-terminal to the gap do not. Hence, the core region for oligomer S appears to start somewhere in the gap region 175–181. In the case of the worm-like fibrils as well as of oligomer L, the core region is mapped to the residues 168–223, but it is less ordered at the two ends of this region for oligomer L than for the worm-like fibrils, as shown by the HDX data for the peptic fragments 168–173, 168–174, and 217–223 (Fig. 3). Another difference is in sequence segment 144–154, for which oligomer S shows relatively more protection compared to oligomer L and worm-like fibrils. The protection in oligomer S is not as high as in the core region. Finally, segment 190–197 is more flexible in oligomer L and the worm-like fibrils than it is in oligomer S (Fig. 3).

Worm-like fibrils possess more ordered structure than do oligomers L and S

Although their patterns of protection against HDX are similar, worm-like fibrils show more protection

than either oligomer L or oligomer S (Fig. 2b). The higher protection in the worm-like fibrils compared to both oligomers indicates an increase in ordered structure with the formation of worm-like fibrils. Increased protection, especially at the boundaries of the core region, clearly indicates an expansion of the core region as the oligomers are converted to worm-like fibrils.

Worm-like fibrils, as well as oligomers L and S, show conformational heterogeneity

A peptide fragment that exists in at least two different conformations in the protein, differing greatly in protection against hydrogen exchange, will display a bimodal isotope distribution in the mass spectrum. Such bimodal isotope mass distributions are seen for sequence segments 109–132, 119–132, and 154–167 derived from either the oligomers or the worm-like fibrils, but not from native moPrP or deuterated moPrP (Fig. 4). Hence, sequence segments 109–132 and 154–167 exist in at least two conformations in each of these aggregate forms. For both structural segments, one population is very weakly protected and gets fully deuterated within 2 h of HDX, while the other conformation is deuterated gradually over 24 h (Fig. 5). Hence, it appears that in some, but not all, molecules of oligomer L and worm-like fibrils, the core region is extended up to residue 154 at its N-terminal end. For oligomer S, the core region is discontinuous in the molecules that are protected in sequence segment 154–167.

Conformational heterogeneity is also evident in a similar manner in sequence segment 32–55 of only the worm-like fibrils (Fig. 4). Hence, some of the protein molecules in the worm-like fibrils possess moderately protective structure in segment 32–55, while other protein molecules are very weakly protected, if at all, against HDX in the same structural region. This region is unstructured in both oligomeric forms.

Figure S6 shows that the fractions of molecules that become deuterated in sequence segments 109–132 and 154–167 increase with the time of exchange. Small fractions (10–20%) of the protein molecules in the worm-like fibrils remain undeuterated in these sequence segments even after 24 h of HDX, while segments of oligomers L and S undergo nearly complete deuteration. Hence, the protective structure in these two sequence segments is more stable in the worm-like fibrils than in the oligomers.

Figure 6 summarizes the results of the HDX experiments. It shows the segments of the sequence that are highly protected, moderately protected, and weakly protected against HDX, and it also shows the sequence segments that are protected in some but not all protein molecules comprising the three aggregates.

Oligomers L and S, as well as the worm-like fibrils, permeabilize lipid membranes

To determine whether any of the three aggregates was capable of disrupting lipid membrane structure, current measurements on BLMs as well as liposome swelling measurements were utilized.

BLM measurements

Addition of monomeric protein (250 nM) into the *cis* compartment of the BLM chamber resulted in step increases in current, corresponding to a unitary

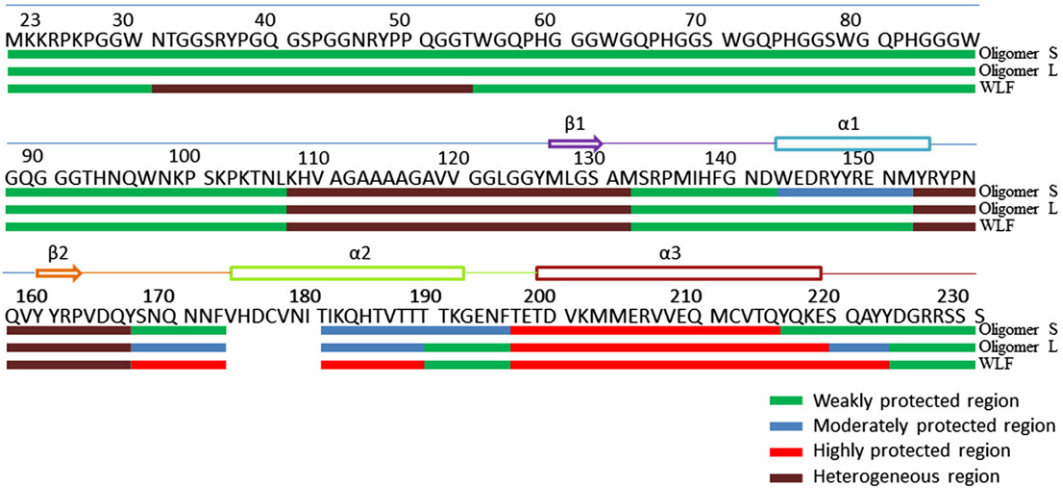

Fig. 6. Correlation of protection against HDX to the sequence of moPrP. Sequence segments highly protected (<25% deuterium incorporation after 24 h of HDX), moderately protected (25–75% deuterium incorporation after 24 h of HDX), and weakly protected (>75% deuterium incorporation after 24 h of HDX) are shown as red, blue, and green lines below the protein sequence, for oligomer S, oligomer L, and the worm-like fibrils (WLF). Also shown as brown lines are the sequence segments exhibiting conformational heterogeneity in the three aggregates.

conductance of 10.02 ± 1.35 pS in 1 M KCl (Fig. 7a). Transitions to both higher and lower conductance are seen at steady state. Addition of preformed aggregates resulted in large step increases in current over 2–30 min after addition. Total membrane current increased monotonically with concentration over the range 50–400 nM (Fig. 7b). High concentrations of all three aggregates resulted in current increases to the point where the amplifier was saturated (Fig. S7a).

Vesicle swelling measurements

Unilamellar liposomes encapsulating 3 mM Dextran (10 kDa) as an impermeant solute, were diluted into isosmotic solutions of PEG (200, 3000 and 8000 Da). Control liposomes showed no change in absorbance on dilution into PEG solution. Liposomes incubated with moPrP aggregates (100 nM) showed rapid decreases in absorbance on dilution into PEG200 (Fig. 7c), indicative of swelling following influx of solute and consequent entry of water. Liposomes incubated with 5 mM monomeric moPrP showed marginal swelling.

The limiting change in absorbance is an index of the fraction of proteoliposomes permeable to the solute. Figure 7d shows that the fraction of proteoliposomes containing large pores increases monotonically with aggregate concentration, with oligomers L and S being more efficacious than worm-like fibrils at the same protein concentration.

Swelling was more extensive on dilution into PEG 200 than into PEG 3000 and marginal on dilution into PEG 8000 (Fig. S7b), indicating that very few proteoliposomes have pores that can pass PEG 8000, and placing an upper limit of 4 nm on pore radius. It may be noted that the dynamic light scattering properties of the liposomes were not significantly affected by incorporation of the proteins (data not shown), indicating that permeabilization of the liposomes was not due to detergent action.

Discussion

Structural core of worm-like fibrils

The structural core of worm-like fibrils formed by moPrP, which encompasses the sequence segment ~168–223 (Fig. 6), is broadly similar to that of straight fibrils made from different recombinant PrP constructs under different conditions, which have

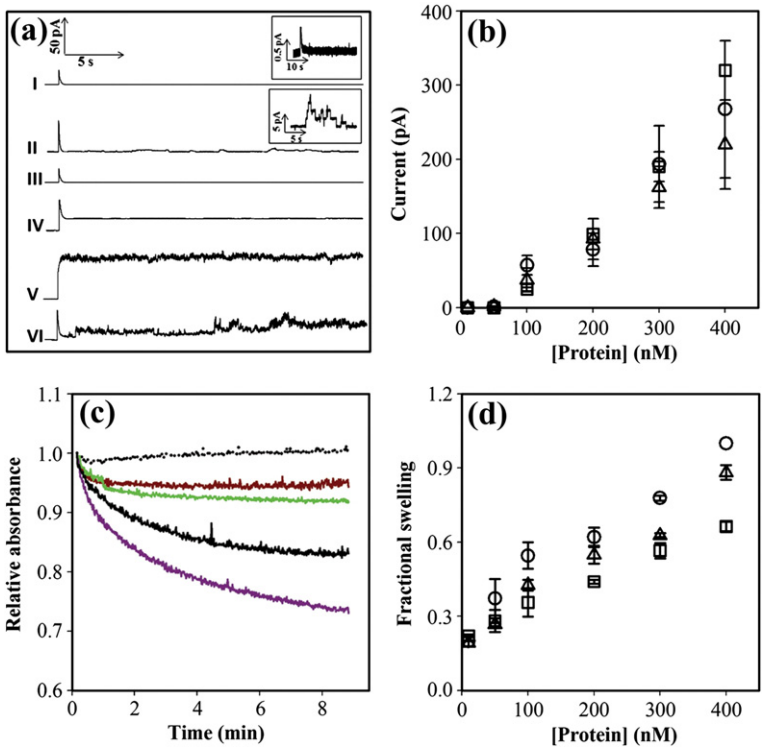

Fig. 7. Comparison of the abilities of moPrP amyloid aggregates to perturb lipid membrane structures. (a and b) Currents in BLMs. (a) presents 30-s traces of current flow through the membrane after adding (I) 50 μL of aggregation buffer, (II) 250 nM monomeric moPrP, (III) 100 nM monomeric moPrP, (IV) 100 nM worm-like fibrils, (V) 100 nM oligomer L, and (VI) 100 nM oligomer S. Current was recorded at +80 mV in all the traces. The insets in (I) and (II) show expanded sections of the recordings. Single channel opening and closing events are seen when 250 nM monomeric moPrP is added to the BLM. The initial spikes in all the recordings are caused by the jump in the applied voltage from 0 to +80 mV. In (b), current through the membrane is plotted against the concentration of the aggregates, (○) oligomer L, (Δ) oligomer S, and (□) worm-like fibrils. (c and d) Liposome swelling monitored by decrease in absorbance at 520 nm. In (c), swelling of liposomes pre-incubated with different aggregates was monitored upon dilution into isosmotic buffer containing PEG 200. Liposomes were pre-incubated with buffer (black dotted line), 5 μM monomeric moPrP (brown line), 100 nM oligomer L (purple line), 100 nM oligomer S (black continuous line), and 100 nM worm-like fibrils (green line). In (d), the fraction of liposomes that underwent swelling is plotted against the concentrations of oligomer L (○), oligomer S (Δ), and worm-like fibrils (□). The liposome swelling data are shown from one batch of liposome preparation (c) and the extents of swelling were calculated from experiments with two batches of liposomes (d).

been studied by solid-state NMR,[10] EPR,[9,12] and HDX measurements.[11,34–37] This result is remarkable because the two types of fibrils are so different in external morphology and size. The principal difference in the HDX-enabled delineation of the core in this study of worm-like fibrils from that in previous studies of straight fibrils[11] is that the core is not continuous in worm-like fibrils, as it is in straight fibrils. Since sequence segment 190–197 appears to be unstructured in the worm-like fibrils, the core of these fibrils appears to be divided into two discontinuous stretches 168–189 and 198–223. The entire region is structured in straight fibrils.[11,36] It is likely that the differences in core structures and stabilities between worm-like and straight fibrils are responsible for the very different morphologies and sizes of these two types of fibrils.[15,32]

Structural model for worm-like fibrils

Of the three models that have been proposed to describe the structure of PrP^{Sc}, the β-helix model[7] has α-helices 2 and 3 of PrP^{C} largely preserved, while the spiral model[8] has all three α-helices retaining their native conformation. A previous Fourier transform infrared study[31] of worm-like fibrils had suggested that worm-like fibrils were devoid of α-helical structure. In the current study, the absence of α-helical structure has been confirmed by the far-UV CD spectra (Fig. S1c), indicating only β-sheet structure. Hence, the structure of worm-like fibrils appears inconsistent with both the β-helix[7] and the spiral model.[8]

The parallel in-register β-sheet model,[9,10] proposed for PrP^{Sc}, postulates conversion of the C-terminal α-helices 2 and 3 in PrP^{C} to β-sheet in PrP^{Sc} together with the unfolding of β-strand 1 and α-helix 1. This model is consistent with the observation that the isolated sequence segment encompassing α-helices 2 and 3 of PrP^{C} can oligomerize and form straight fibrils.[38,39] In the current study, the delineation of the structural core of worm-like fibrils to sequence segment ~168–223 (Fig. 6), which also forms the structural core of straight fibrils,[9–12,34–37] not only is consistent with this model but also appears to be inconsistent with both the β-helix model[7] and the spiral model.[8] The latter two models propose cores encompassing residue segments 89–175 and 116–164, respectively. It should be noted that while the structural core of worm-like fibrils appears to be a β-sheet, and not a β-helix or a spiral in which α-helices are retained, it is not known at present whether the arrangement of this β-sheet is parallel in-register or something else.

Core regions of the oligomers and worm-like fibrils show similarities and differences

This is the first characterization of oligomers that form initially during the course of fibril formation by the prion protein. It is shown that the structural core of the worm-like fibrils is similar not only to that of oligomer L from which they arise but also to that of the off-pathway oligomer S. Oligomer S is, however, different from the other two aggregates in the following respects: (1) its core region is shorter and less stable at its N-terminal end. Indeed, CD measurements show that there is less β-sheet structure in oligomer S than in oligomer L (Fig. S1c); (2) its sequence segment 190–197 is structured, and hence its basic core region is continuous; and (3) sequence segment 144–154 adopts moderately protective structure. At present, it is not known which of these differences is responsible for oligomer S not being able to form fibrils. It is possible that sequence segment 144–154 retains α-helix 1 of native protein, and this disallows its further growth.

Transformation of oligomer L into worm-like fibrils involves core expansion

Previous studies of moPrP aggregation using multiple probes had shown that much of the α-helix to β-sheet conformational conversion takes place during the formation of oligomers itself[20,31] and that the β-structure is consolidated as oligomer L transforms into worm-like fibrils.[32] In this study, the internal changes taking place during the transformation of oligomer L into worm-like fibrils have been delineated. More protection against HDX is seen at the boundaries of the core region in the worm-like fibrils than in the on-pathway oligomer L. In particular, the basic core region of the highly protected structure is shorter at its N-terminal end in oligomer L (Fig. 6). This clearly indicates that the core region expands as oligomer L transforms into worm-like fibrils. In the case of the amyloid-β peptide, Aβ40, such an expansion of the core region has been shown to happen as oligomers[40] and protofibrils[41,42] transform into less-toxic fibrils. It remains to be seen whether the worm-like fibrils are less toxic than oligomer L.

Conformational heterogeneity increases as oligomers convert into worm-like fibrils

A major advantage of using HDX–MS measurements over NMR or EPR to characterize structure is that different coexisting conformations can be identified because they manifest bimodal mass distributions.[43] It should be noted that the bimodal isotope distribution patterns observed in three fragments of the aggregates are not attributable to uncorrelated HDX occurring in local structural regions in aggregate molecules under the quench conditions (pH 2.5, 4 °C), because such patterns are not observed for the same three fragments derived from native moPrP or deuterated moPrP that were also subjected to exactly the same quench conditions

as were the aggregates (Fig. 5). Moreover, even for the same three fragments derived from the aggregates, the isotope pattern becomes unimodal when the aggregates are allowed to undergo HDX for longer times prior to quenching (see above), whereas if uncorrelated HDX had occurred into local structural segments of the aggregates under the quench conditions, such back exchange would still have led to the observation of a bimodal pattern independent of the labeling time. Indeed, it is very unlikely, in the first place, that the HDX mechanism would shift from the EX2 limit to the EX1 limit[44] in any local region of the aggregated molecules under the quench conditions, because the aggregates were made to unfold completely at the same time HDX was quenched (see Materials and Methods), and the intrinsic HDX rate ($\sim 10^{-4}$ s^{-1}) is more than 200-fold slower than the rate at which the aggregates unfold (~ 0.02 s^{-1}) under the quench/unfolding conditions.

The observation (Fig. 4) that sequence segments 109–132 and 154–167 adopt multiple conformations in all three amyloid aggregates, and that sequence segment 32–55 does so only in the worm-like fibrils, suggests that all three aggregates can adopt multiple conformations that differ in at least one of these three distinct structural regions. The conformational heterogeneity in all three aggregates suggests that protein molecules in each of these aggregates possess different extents of protective structure, presumably β-sheet structure as indicated by the CD spectra (Fig. S1c), at different locations in their sequence. It remains to be determined whether each aggregate assembly consists of differently structured protein molecules, or whether individual aggregate assemblies always consist of protein molecules in the same conformation.

Until now, most structural studies of PrP amyloid have been carried out with N-terminal truncated variants of the protein; consequently, structural information about the N-terminal half of the protein in amyloid fibrils is sparse. In this study, the observation that sequence segment 32–55 adopts structure in a small but significant fraction of the worm-like fibrils suggests that the N-terminal half of the protein sequence may have malleable structure that could impart it important functional roles.

Conformational heterogeneity in the different aggregation states is believed to be responsible for the prion strain phenomenon.[16] Different strains of transmissible spongiform encephalopathy are linked to conformational differences within the PrP^{Sc} isoform.[14,45,46] The localization of the conformational heterogeneity to two sequence segments of the protein for all three amyloid aggregates, and additionally to sequence segment 32–55 for only the worm-like fibrils (Fig. 6), will be important for understanding how conformational heterogeneity arises from the same protein sequence under identical environmental conditions.

Similarity of worm-like fibrils to mouse brain-derived PrP^{Sc}

An HDX study of authentic mouse-brain derived PrP^{Sc} (Ref. 37) had indicated that its structural core, encompassing the sequence segment 90–230, was extended compared to that of straight fibrils formed by any recombinant prion protein. The present study of worm-like fibrils suggests that in at least some of the fibril protein molecules, the structural core may be longer than that of the straight fibrils and about as long as that in PrP^{Sc} (Ref. 37). Moderate to strong protection is also observed in sequence segments 109–132 and 154–167 of the worm-like fibrils, suggesting that in at least some of these fibrils, the structural core comprises the sequence segment 109–223, interrupted by two unstructured regions (Fig. 6). It is therefore not surprising that a Met-to-Val mutation at residue position 129 has been shown to modulate the pathology of prion disease and inter-oligomer interactions,[47] as well as the stability of oligomer L, and the rate of transformation of oligomer L into worm-like fibrils.[32] It appears that the worm-like fibrils formed at acidic pH may be a better model for PrP^{Sc} than fibrils formed under other conditions.

Syrian hamster brain-derived PrP^{Sc}-seeded PMCA aggregates and worm-like fibrils, but not straight fibrils formed spontaneously from recombinant proteins,[36] are also similar in displaying conformational heterogeneity for sequence segments 109–132 and 154–167 (see above). The similarities in structure and heterogeneity between worm-like fibrils and PrP^{Sc} are especially striking, given the differences that have been observed[37,48] between straight fibrils formed by recombinant PrP and brain-derived PrP^{Sc}.

Putative toxicity of the oligomers and worm-like fibrils

Monomeric moPrP at high concentrations (250 nM) forms well-defined pores in BLM with a unitary conductance of ~10 pS, which is somewhat lower than that reported for fragments of Syrian hamster PrP[49] and is also lower than the conductance of plasma membrane ion channels. While this demonstrates a nascent capability of membrane insertion, this small-conductance pore was essentially impermeable to PEG. moPrP aggregates, on the other hand, form pores of nanoSiemen conductance, but smaller than 4 nm in radius, at the same concentrations, and either larger or more numerous pores at higher concentrations (Fig. 7). It may be noted that pores of this dimension are toxic to cells, with just a few pores sufficing for lethality.[50] It is difficult to compare the efficiencies of the various aggregates to form such pores inasmuch as the number concentrations of the different aggregates are impossible to estimate.

Amyloid aggregates of other proteins also similarly permeabilize membranes[51,52] and are toxic to cells.[53,54] It is intriguing that the three amyloid aggregates of moPrP, which differ drastically in size and morphology, are all capable of disrupting membrane structure (Fig. 7). This suggests that features shared by the three aggregates are responsible for this activity. An obvious candidate is the common C-terminal core shared by the three aggregates. The other possibility is the unstructured N-terminal half of the sequence, which was shown to interact with membranes and become structured in the case of monomeric PrP.[55] This interaction may be responsible for the ability of monomeric PrP to form well-defined pores (Fig. 7a). The unstructured N-terminal half of the sequence was also shown to become structured when straight fibrils were formed in the presence of membranes.[35] The three amyloid aggregates studied here cause a several 100-fold greater increase in membrane permeability than does monomeric PrP. Current studies are targeted towards understanding how the mechanisms of membrane permeabilization are different for the aggregates and the monomer.

Materials and Methods

Protein expression and purification

The moPrP was expressed and purified as described previously.[20] The purified protein was transferred to Milli-Q water using an Amicon ultrafiltration cell, lyophilized, and stored at −20 °C.

Preparation and separation of oligomers and fibrils

β-Rich oligomer and fibrils were prepared, and individual oligomers L and S were purified, as described previously.[32] The aggregation buffer was 50 mM glycine buffer containing 150 mM NaCl at pH 2. Worm-like fibrils were formed by incubation of the β-rich oligomer at 50 °C for 3 h.

Fluorescence, CD, and AFM assays

ThT fluorescence assays and AFM measurements were carried out as described previously.[20] For intrinsic fluorescence and far-UV CD measurements, the protein concentrations used were 5 μM and 10 μM, respectively.

Static and dynamic light scattering measurements

Simultaneous measurements of static light scattering at seven angles and dynamic light scattering were performed using a DAWN 8+, eight-angle light scattering instrument (Wyatt Technology Corp., Santa Barbara, CA). For determining mass and hydrodynamic radius of oligomer S and oligomer L, purified oligomers were diluted to 2 μM in aggregation buffer and run through a 0.02-μm filter at a constant rate into the light scattering fused silica flow cell. For aggregation kinetics, the reaction was set at a temperature of 50 °C and a protein concentration of 25 μM; aliquots were taken out at different time points, diluted to 1.5 μM, and run through a 0.1-μm filter at a constant rate into the flow cell. Data were analyzed using the software Astra. Normalization of the scattering intensity was done using a solution of bovine serum albumin.

Peptide mapping

To generate a peptide map of moPrP, the protein, in 10 mM sodium acetate buffer at pH 4.0, was subjected to on-line pepsin digestion in 0.05% formic acid using an immobilized pepsin cartridge (Applied Biosystems) at a flow rate of 50 μL/min on a nanoAcquity UPLC (Waters). The eluted peptides were collected using a peptide trap column (C18 reversed-phase chromatography column), washed to remove salt, and eluted on an analytical C18 reversed-phase chromatography column using a gradient of 3–40% acetonitrile (0.1% formic acid) at a flow rate of 45 μL/min. The peptides were directed to the coupled Synapt G2 HD mass spectrometer (Waters). The peptides were sequenced using the MS/tandem MS (MS^E) method, followed by analysis with the ProteinLynx Global Server software (Waters) and manual inspection.

HDX–MS measurements

Purified oligomers were concentrated to 300 μM by centrifugation (10,000*g*) through 10-kDa molecular mass cutoff filters. To initiate deuterium labeling, 50 μL of oligomers were diluted into 0.95 mL of aggregation buffer prepared in D_2O (pH 2.0, corrected for isotope effect) and incubated it at 25 °C. At various time points of labeling, aliquots of 200 μL were taken out and mixed with 400 μL of ice-cold 7.0 M guanidine hydrochloride (GdnHCl) under exchange-quenched conditions (100 mM glycine, pH 2.5) to dissolve oligomers. After 1 min of incubation, the samples were desalted using a Sephadex G-25 HiTrap desalting column equilibrated with water at pH 2.5 in conjunction with an Akta Basic HPLC. The desalted samples were injected into the HDX module (Waters) coupled with the nanoAcquity UPLC, for online pepsin digestion with immobilized pepsin cartridge at a flow rate of 50 μL/min of water (0.05% formic acid). The peptides eluted from the pepsin cartridge were collected using the peptide trap column, washed to remove salt and eluted on an analytical C18 reversed-phase chromatography column with a gradient of 3–40% acetonitrile (0.1% formic acid) at a flow rate of 45 μL/min (total elution time of 10 min). All columns were kept at 4 °C in the cooling chamber of the HDX module. The peptides separated on the column were detected using the Synapt G2 HD mass spectrometer. The mass spectrometer parameters were as follows: source temperature, 35 °C; desolvation temperature, 100 °C; capillary voltage, 3.0 kV.

Worm-like fibrils formed at 50 °C were concentrated to 300 μM by centrifugation (5000*g*) using a 300-kDa molecular mass cutoff filter. Deuterium labeling was started by diluting 50 μL of worm-like fibrils in 0.95 mL of aggregation buffer prepared in D_2O (pH 2.0, corrected for isotope effect) and incubating at 25 °C. Afterwards, worm-like fibrils were processed in the same way, as were oligomer L

and oligomer S. Exchange experiments of native moPrP were also carried out in a similar way after 20-fold dilution of protein in 10 mM sodium acetate, prepared in D_2O (pH 4.0, corrected for isotope effect). To mimic the digestion conditions of oligomers and fibrils, 200 μL of D_2O-labeled sample was taken and mixed it with 400 μL of ice-cold 7.0 M GdnHCl under exchange-quenched conditions (100 mM glycine, pH 2.5), and processed it in the same way as the oligomers and worm-like fibrils.

Peptide masses were calculated from the centroid of the isotopic envelope using MassLynx software, and the shift in mass of labeled peptides relative to unlabeled peptides was used to determine the extent of deuterium incorporation at each time point of hydrogen exchange. As the sample was in 95% D_2O during labeling and was exposed to H_2O after dissolution in GdnHCl, control experiments were carried out to correct for the back exchange and forward exchange. To this end, moPrP was incubated in 10 mM sodium acetate, pH 4.0 (95% D_2O), and deuterated by unfolding at 65 °C for 10 min followed by refolding on ice. Refolded moPrP was shown to behave like native moPrP, using CD spectroscopy and thermal equilibrium unfolding studies (data not shown). The fully deuterated moPrP sample was processed in the same way as the oligomers and worm-like fibrils. The extent of deuterium incorporation in each peptide, % D, was determined using the equation $\%\ D = (m(t) - m(0\%))/(m(95\%) - m(0\%)) \times 100$, where $m(t)$ is the measured centroid mass of the peptide at time point t, $m(0\%)$ is the measured mass of an undeuterated reference sample, and $m(95\%)$ is the measured mass of a fully deuterated reference sample (in 95% D_2O).

The percent deuterium incorporation for peptides showing a bimodal distribution was calculated from the weighted average deuterium incorporation of protected and accessible species. For calculation of the percent protected and accessible forms for a peptide, the bimodal isotopic peaks were fitted to the individual isotopic peak as a sum of Gaussian distributions using OriginPro 8. The relative percentage of each form was calculated from the relative area under each peak.

Preparation of unilamellar liposomes and the liposome swelling assay

Unilamellar liposomes were made from diphytanoylphosphatidylcholine (DPhPC) in aggregation buffer containing 3 mM dextran (10 kDa), as described earlier.[56] Dynamic light scattering measurements on a DynaPro-99 instrument (Protein Solutions) indicated that the average diameter of the vesicles was 460 ± 65 nm. Liposomes were subsequently incubated with moPrP aggregates for 1 h before performing the liposome swelling assay.

The pore-forming activity of moPrP aggregates was assessed by a liposome swelling assay.[56] The dextran-containing liposomes were diluted into buffer containing different PEGs (200, 3000, and 8000 Da), and the absorbance at 520 nm was recorded at 1-s intervals for 10 min using a Cary 1 UV–Visible spectrophotometer (Varian). Buffer conditions under which no absorbance change was seen with control liposomes were deemed isosmotic. The liposome mixture was stirred constantly to prevent settling and aggregation. Influx of solute into proteoliposomes results in swelling and consequent decrease in absorbance. The limiting change in absorbance is proportional to the fraction of proteoliposomes that are permeable to the solute.

Planar BLM experiments

Planar bilayers were made from monolayers by a modification of the technique of Montal and Mueller.[57] Briefly, a 100-μm aperture in a thin Teflon membrane separating two Teflon chambers was painted with hexadecane in *n*-pentane (1:9 v/v). Monolayers of equal amounts of diphytanoylphosphatidylcholine (25 mg/mL in *n*-pentane) and cholesterol (25 mg/mL in diethyl ether) were spread on buffer containing 1 M KCl, 5 mM $CaCl_2$, and 50 mM glycine–HCl (pH 2.0) in both chambers. Lipid bilayers were formed by slowly lowering and raising the solution level past the aperture. Bilayer formation was followed by monitoring conductance and capacitance. Before adding moPrP aggregates to the membrane, membrane stability and conductance were monitored at +100 mV for 2–3 h. Proteins were added to the *cis* chamber, which was stirred with a magnetic stirrer, and insertion of pores was assessed by monitoring current at a holding potential of +80 mV. Voltage-clamp recording was performed using a BC-525C bilayer clamp amplifier (Warner Instruments). Analogue data from the amplifier filtered at 1 kHz were digitized with a Digidata 1322 (Axon Instruments) at 10 kHz. pCLAMP 10 (Axon Instruments) was used to generate voltage-clamp commands, acquire membrane currents, and analyze digitized data.

Acknowledgements

We thank members of our laboratory for discussion and for their comments on the manuscript. We thank S. Jain for assistance in peptide mapping. The AFM images were collected at the Central Imaging Facility of the National Centre for Biological Sciences. J.B.U. is a recipient of a JC Bose National Fellowship from the Government of India. A.T.S. is a recipient of a Junior Research Fellowship from the Council of Scientific and Industrial Research, Government of India. This work was funded by the Tata Institute of Fundamental Research, and by the Department of Biotechnology, Government of India.

Supplementary Data

Supplementary data to this article can be found online at http://dx.doi.org/10.1016/j.jmb.2012.06.040

References

1. Griffith, J. S. (1967). Self-replication and scrapie. *Nature*, **215**, 1043–1044.
2. McKinley, M. P., Bolton, D. C. & Prusiner, S. B. (1983). A protease-resistant protein is a structural component of the scrapie prion. *Cell*, **35**, 57–62.

3. Prusiner, S. B. (1997). Prion diseases and the BSE crisis. *Science*, **278**, 245–251.
4. Prusiner, S. B. (1998). Prions. *Proc. Natl Acad. Sci. USA*, **95**, 13363–13383.
5. Aguzzi, A. & Polymenidou, M. (2004). Mammalian prion biology: one century of evolving concepts. *Cell*, **116**, 313–327.
6. Diaz-Espinoza, R. & Soto, C. (2012). High-resolution structure of infectious prion protein: the final frontier. *Nat. Struct. Mol. Biol.* **19**, 370–377.
7. Govaerts, C., Wille, H., Prusiner, S. B. & Cohen, F. E. (2004). Evidence for assembly of prions with left-handed beta-helices into trimers. *Proc. Natl Acad. Sci. USA*, **101**, 8342–8347.
8. DeMarco, M. L. & Daggett, V. (2007). Molecular mechanism for low pH triggered misfolding of the human prion protein. *Biochemistry*, **46**, 3045–3054.
9. Cobb, N. J., Sonnichsen, F. D., McHaourab, H. & Surewicz, W. K. (2007). Molecular architecture of human prion protein amyloid: a parallel, in-register beta-structure. *Proc. Natl Acad. Sci. USA*, **104**, 18946–18951.
10. Tycko, R., Savtchenko, R., Ostapchenko, V. G., Makarava, N. & Baskakov, I. V. (2010). The α-helical C-terminal domain of full-length recombinant PrP converts to an in-register parallel β-sheet structure in PrP fibrils: evidence from solid state nuclear magnetic resonance. *Biochemistry*, **49**, 9488–9497.
11. Lu, X., Wintrode, P. L. & Surewicz, W. K. (2007). β-Sheet core of human prion protein amyloid fibrils as determined by hydrogen/deuterium exchange. *Proc. Natl Acad. Sci. USA*, **104**, 1510–1515.
12. Cobb, N. J., Apetri, A. C. & Surewicz, W. K. (2008). Prion protein amyloid formation under native-like conditions involves refolding of the C-terminal α-helical domain. *J. Biol. Chem.* **283**, 34704–34711.
13. Kumar, J., Sreeramulu, S., Schmidt, T. L., Richter, C., Vonck, J., Heckel, A. *et al.* (2010). Prion protein amyloid formation involves structural rearrangements in the C-terminal domain. *ChemBioChem*, **11**, 1208–1213.
14. Caughey, B., Raymond, G. J. & Bessen, R. A. (1998). Strain-dependent differences in β-sheet conformations of abnormal prion protein. *J. Biol. Chem.* **273**, 32230–32235.
15. Jain, S. & Udgaonkar, J. B. (2011). Prion protein aggregation. *Curr. Sci.* **101**, 1311–1327.
16. Toyama, B. H. & Weissman, J. S. (2011). Amyloid structure: conformational diversity and consequences. *Annu. Rev. Biochem.* **80**, 557–585.
17. Legname, G., Baskakov, I. V., Nguyen, H. B., Riesner, D., Cohen, F. E., DeArmond, S. J. *et al.* (2004). Synthetic mammalian prions. *Science*, **305**, 673–676.
18. Cobb, N. J. & Surewicz, W. K. (2009). Prion diseases and their biochemical mechanisms. *Biochemistry*, **48**, 2574–2585.
19. Baskakov, I. V., Legname, G., Baldwin, M. A., Prusiner, S. B. & Cohen, F. E. (2002). Pathway complexity of prion protein assembly into amyloid. *J. Biol. Chem.* **277**, 21140–21148.
20. Jain, S. & Udgaonkar, J. B. (2008). Evidence for stepwise formation of amyloid fibrils by the mouse prion protein. *J. Mol. Biol.* **382**, 1228–1241.
21. Lashuel, H. A., Hartley, D., Petre, B. M., Walz, T. & Lansbury, P. T., Jr (2002). Amyloid pores from pathogenic mutations. *Nature*, **418**, 291.
22. Ferreira, S. T., Vieira, M. N. & De Felice, F. G. (2007). Soluble protein oligomers as emerging toxins in Alzheimer's and other amyloid diseases. *IUBMB Life*, **59**, 332–345.
23. Outeiro, T. F., Putcha, P., Tetzlaff, J. E., Spoelgen, R., Koker, M., Carvalho, F. *et al.* (2008). Formation of toxic oligomeric α-synuclein species in living cells. *PLoS One*, **3**, e1867.
24. Xue, W. F., Hellewell, A. L., Gosal, W. S., Homans, S. W., Hewitt, E. W. & Radford, S. E. (2009). Fibril fragmentation enhances amyloid cytotoxicity. *J. Biol. Chem.* **284**, 34272–34282.
25. Silveira, J. R., Raymond, G. J., Hughson, A. G., Race, R. E., Sim, V. L., Hayes, S. F. *et al.* (2005). The most infectious prion protein particles. *Nature*, **437**, 257–261.
26. Novitskaya, V., Makarava, N., Bellon, A., Bocharova, O. V., Bronstein, I. B., Williamson, R. A. *et al.* (2006). Probing the conformation of the prion protein within a single amyloid fibril using a novel immunoconformational assay. *J. Biol. Chem.* **281**, 15536–15545.
27. Kazlauskaite, J., Young, A., Gardner, C. E., Macpherson, J. V., Venien-Bryan, C. & Pinheiro, T. J. T. (2005). An unusual soluble β-turn-rich conformation of prion is involved in fibril formation and toxic to neuronal cells. *Biochem. Biophys. Res. Commun.* **328**, 292–305.
28. Simoneau, S., Rezaei, H., Sales, N., Kaiser-Schulz, G., Lefebvre-Roque, M., Vidal, C. *et al.* (2007). In vitro and in vivo neurotoxicity of prion protein oligomers. *PLoS Pathog.* **3**, e125.
29. Mallucci, G., Dickinson, A., Linehan, J., Klohn, P., Brandner, S. & Collinge, J. (2003). Depleting neuronal PrP in prion infection prevents disease and reverses spongiosis. *Science*, **302**, 871–874.
30. Khan, M. Q., Sweeting, B., Mulligan, V. K., Arslan, P. E., Cashman, N. R., Pai, E. F. *et al.* (2010). Prion disease susceptibility is affected by β-structure folding propensity and local side-chain interactions in PrP. *Proc. Natl Acad. Sci. USA*, **107**, 19808–19813.
31. Jain, S. & Udgaonkar, J. B. (2010). Salt-induced modulation of the pathway of amyloid fibril formation by the mouse prion protein. *Biochemistry*, **49**, 7615–7624.
32. Jain, S. & Udgaonkar, J. B. (2011). Defining the pathway of worm-like amyloid fibril formation by the mouse prion protein by delineation of the productive and unproductive oligomerization reactions. *Biochemistry*, **50**, 1153–1161.
33. Lee, Y. J., Savtchenko, R., Ostapchenko, V. G., Makarava, N. & Baskakov, I. V. (2011). Molecular structure of amyloid fibrils controls the relationship between fibrillar size and toxicity. *PLoS One*, **6**, e20244.
34. Eghiaian, F., Daubenfeld, T., Quenet, Y., van Audenhaege, M., Bouin, A. P., van der Rest, G. *et al.* (2007). Diversity in prion protein oligomerization pathways results from domain expansion as revealed by hydrogen/deuterium exchange and disulfide linkage. *Proc. Natl Acad. Sci. USA*, **104**, 7414–7419.
35. Nazabal, A., Hornemann, S., Aguzzic, A. & Zenobia, R. (2009). Hydrogen/deuterium exchange mass spectrometry identifies two highly protected regions in

recombinant full-length prion protein amyloid fibrils. *J. Mass Spectrom.* **44**, 965–977.
36. Smirnovas, V., Kim, J., Lu, X., Atarashi, R., Caughey, B. & Surewicz, W. K. (2009). Distinct structures of scrapie prion protein (PrP^{Sc})-seeded *versus* spontaneous recombinant prion protein fibrils revealed by hydrogen/deuterium exchange. *J. Biol. Chem.* **284**, 24233–24241.
37. Smirnovas, V., Baron, G. S., Offerdahl, D. K., Raymond, G. J., Caughey, B. & Surewicz, W. K. (2011). Structural organization of brain-derived mammalian prions examined by hydrogen–deuterium exchange. *Nat. Struct. Mol. Biol.* **18**, 504–506.
38. Chakroun, N., Prigent, S., Dreiss, C. A., Noinville, S., Chapuis, C., Fraternali, F. *et al.* (2010). The oligomerization properties of prion protein are restricted to the H2H3 domain. *FASEB J.* **24**, 3222–3231.
39. Adrover, M., Pauwels, K., Prigent, S., de Chiara, C., Xu, Z., Chapuis, C. *et al.* (2010). Prion fibrillization is mediated by a native structural element that comprises helices H2 and H3. *J. Biol. Chem.* **285**, 21004–21012.
40. Zhang, A., Qi, W., Good, T. A. & Fernandez, E. J. (2009). Structural differences between Aβ (1–40) intermediate oligomers and fibrils elucidated by proteolytic fragmentation and hydrogen/deuterium exchange. *Biophys. J.* **96**, 1091–1104.
41. Kheterpal, I., Lashuel, H. A., Hartley, D. M., Walz, T., Lansbury, P. T., Jr & Wetzel, R. (2003). A-beta protofibrils possess a stable core structure resistant to hydrogen exchange. *Biochemistry*, **42**, 14092–14098.
42. Kheterpal, I., Chen, M., Cook, K. D. & Wetzel, R. (2006). Structural differences in Aβ amyloid protofibrils and fibrils mapped by hydrogen exchange–mass spectrometry with on-line proteolytic fragmentation. *J. Mol. Biol.* **361**, 785–795.
43. Wani, A. H. & Udgaonkar, J. B. (2009). Native state dynamics drive the unfolding of the SH3 domain of PI3 kinase at high denaturant concentration. *Proc. Natl Acad. Sci. USA*, **106**, 20711–20716.
44. Wani, A. H. & Udgaonkar, J. B. (2012). Mass spectrometry studies of protein folding. *Curr. Sci.* **102**, 245–265.
45. Telling, G. C., Parchi, P., DeArmond, S. J., Cortelli, P., Montagna, P., Gabizon, R. *et al.* (1996). Evidence for the conformation of the pathologic isoform of the prion protein enciphering and propagating prion diversity. *Science*, **274**, 2079–2082.
46. Thomzig, A., Spassov, S., Friedrich, M., Naumann, D. & Beekes, M. (2004). Discriminating scrapie and bovine spongiform encephalopathy isolates by infrared spectroscopy of pathological prion protein. *J. Biol. Chem.* **279**, 33847–33854.
47. Gerber, R., Voitchovsky, K., Mitchel, C., Tahiri-Alaoui, A., Ryan, J. F., Hore, P. J. *et al.* (2008). Inter-oligomer interactions of the human prion protein are modulated by the polymorphism at codon 129. *J. Mol. Biol.* **381**, 212–220.
48. Wille, H., Bian, W., McDonald, M., Kendall, A., Colby, D. W., Bloch, L. *et al.* (2009). Natural and synthetic prion structure from X-ray fiber diffraction. *Proc. Natl Acad. Sci. USA*, **106**, 16990–16995.
49. Paulis, D., Maras, B., Schininà, M. E., di Francesco, L., Principe, S., Galeno, R. *et al.* (2011). The pathological prion protein forms ionic conductance in lipid bilayer. *Neurochem. Int.* **59**, 168–174.
50. Menestrina, G., Serra, M. D., Comai, M., Coraiola, M., Viero, G., Werner, S. *et al.* (2003). Ion channels and bacterial infection: the case of β-barrel pore forming protein toxins of *Staphylococcus aureus*. *FEBS Lett.* **552**, 54–60.
51. Kayed, R., Sokolov, Y., Edmonds, B., McIntire, T. M., Milton, S. C., Hall, J. E. *et al.* (2004). Permeabilization of lipid bilayers is a common conformation-dependent activity of soluble amyloid oligomers in protein misfolding diseases. *J. Biol. Chem.* **279**, 46363–46366.
52. Last, N. B., Rhoades, E. & Miranker, A. D. (2011). Islet amyloid polypeptide demonstrates a persistent capacity to disrupt membrane integrity. *Proc. Natl Acad. Sci. USA*, **108**, 9460–9465.
53. Demuro, A., Mina, E., Kayed, R., Milton, S. C., Parker, I. & Glabe, C. G. (2005). Calcium dysregulation and membrane disruption as a ubiquitous neurotoxic mechanism of soluble amyloid oligomers. *J. Biol. Chem.* **280**, 17294–17300.
54. Glabe, G. C. (2006). Common mechanisms of amyloid oligomer pathogenesis in degenerative disease. *Neurobiol. Aging*, **27**, 570–575.
55. Morillas, M., Swietnicki, W., Gambetti, P. & Surewicz, W. K. (1999). Membrane environment alters the conformational structure of the recombinant human prion protein. *J. Biol. Chem.* **274**, 36859–36865.
56. Godbole, A., Mitra, R., Dubey, A. K., Reddy, P. S. & Mathew, M. K. (2011). Bacterial expression, purification and characterization of a rice voltage-dependent, anion-selective channel isoform, OsVDAC4. *J. Membr. Biol.* **244**, 67–80.
57. Montal, M. & Mueller, P. (1972). Formation of bimolecular membranes from lipid monolayers and a study of their electrical properties. *Proc. Natl Acad. Sci. USA*, **69**, 3561–3566.